A Finite Strain Elastic Visco-Plastic Consolidation Model for Layered Soft Soils Considering Self-Weight and Nonlinear Creep

By

Ding-Bao Song, Ph.D., Postdoctoral Fellow

Department of Civil and Environmental Engineering

The Hong Kong Polytechnic University, Hong Kong, China. Email: dingbao.song@polyu.edu.hk or dingbao_song@126.com

Kai Lou, Ph.D. Candidate

Department of Civil and Environmental Engineering

The Hong Kong Polytechnic University, Hong Kong, China. Email: kai.lou@connect.polyu.hk

Jian-Hua Yin, Ph.D., Chair Professor

Department of Civil and Environmental Engineering

Research Institute for Land and Space

The Hong Kong Polytechnic University, Hong Kong, China. Email: jian-hua.yin@polyu.edu.hk

Patrick J. Fox, Ph.D., Shaw Professor and Department Head, F.ASCE

Department of Civil and Environmental Engineering

Pennsylvania State University, University Park, PA 16802. Email: pjfox@engr.psu.edu

Wen-Bo Chen, Ph.D., Research Assistant Professor (corresponding author)

Department of Civil and Environmental Engineering

The Hong Kong Polytechnic University, Hong Kong, China. Email: wb.chen@polyu.edu.hk

Abstract: This paper presents a numerical model, called CS-EVP, for the consolidation of layered soft soils, including soil self-weight and time-dependent compressibility effects. CS-EVP was developed using the piecewise-linear method for large strain consolidation and elastic visco-plastic model for time-dependent soil compressibility. The model accounts for vertical strain, soil self-weight, nonlinear hydraulic conductivity and compressibility, nonlinear creep with limited creep strain, and time-dependent surcharge and/or vacuum loading for layered heterogeneous soils. The accuracy of CS-EVP is verified by comparing calculated values with the results from finite element simulations and a large-scale laboratory vacuum consolidation test of soft soil slurry. Lastly, simulated settlements and excess pore pressure profiles are compared with field measurements for embankment loading in Väsby, Sweden. The results indicate that CS-EVP provides good estimates of long-term large-strain consolidation under both laboratory and field conditions.

Keywords: Layered soil; Finite strain; Consolidation; Elastic visco-plastic; Nonlinear creep; Piecewise-linear.

Introduction

The subsurface conditions for many coastal cities and land development sites often include thick layers of soft compressible soil (Shen et al. 2005; Feng et al. 2021). Similar materials (e.g., dredged slurry) also are used for offshore land reclamation due to the increasing cost and shortage of high-quality granular fill (Chu et al. 2009). In such cases, preloading methods involving surcharge, vacuum, or both, are used to increase the strength and stiffness of soft soil materials over a wide area. The design of a preloading treatment requires estimates of in situ pore pressures and settlement through time and still presents a challenge, especially when long-term secondary compression must be predicted.

The classical Terzaghi (1925) theory for soil consolidation, widely used in practice, assumes small vertical strain, constant hydraulic conductivity, and linear and time-independent compressibility for the soil and provides an analytical solution for the rate of consolidation of a single soil layer under instantaneous surcharge loading. Based on similar assumptions, analytical solutions for the consolidation of layered soils were presented by Schiffman and Stein (1970). Lee et al. (1992) dispensed with the combined parameter of coefficient of consolidation and developed an analysis based on independent parameters for soil compressibility and hydraulic conductivity. Other valuable contributions, including models with depth-dependent ramp loading (Zhu and Yin 1999a), variable soil compressibility (Xie et al. 2002), and new solution methods for consolidation equations (Chen et al. 2005; Hazzard et al. 2008; Kim and Mission 2011), also have been developed for consolidation analysis of layered soils.

Finite strain consolidation theory was developed to account for changing layer thickness during the consolidation process, which can be important for soft soils. General mathematical expressions based on material coordinates were presented by Gibson et al. (1967) and include nonlinear soil compressibility and hydraulic conductivity. Based on this approach, methods were developed to incorporate soil self-weight (Gibson et al. 1981; Lee and Sills 1981) and staged loading (Cargill 1984), and fully explicit analytical solutions were presented by Xie and Leo (2004). Finite strain consolidation analysis also has been conducted using alternate approaches, such as the finite element method (Carter et al. 1979), multiplicative decomposition technique (Borja and Alarcón 1995; Borja et al. 1998; Zhao and Borja 2020), and piecewise-linear method (Yong et al. 1983; Townsend and McVay 1990; Fox and Berles 1997). Of these, the piecewise-linear models are more flexible in terms of initial conditions, boundary conditions, spatial nonlinearity, and material heterogeneity. Fox and Berles (1997) proposed the piecewise-linear finite strain model CS2 for the one-dimensional consolidation of a single soil layer, with further enhancements presented by Fox and Pu (2012). Based on the CS2 method, a series of models have been developed to include the treatment of accreting soil layers (Fox 2000), radial consolidation (Fox et al. 2003), centrifuge conditions (Fox et al. 2005), coupled consolidation and solute transport (Fox 2007; Fox and Lee 2008), constant strain rate (Pu et al. 2013), electro-osmotic consolidation (Zhou et al. 2013), consolidation and solute transport in layered soil systems (Fox et al. 2014; Pu and Fox 2015), and consolidation of unsaturated soils (Qi et al. 2017; Qi et al. 2020). The development of these models provides a reliable basis for simulation of a wide range of large-strain consolidation conditions. Most finite strain consolidation models assume time-independent soil compressibility. Gheisari et al. (2021, 2022) incorporated elastic visco-plastic constitutive equations into the large-strain consolidation framework presented by Qi et al. (2017, 2020) to model the consolidation and creep behaviors of saturated oil sands tailings under self-weight loading; however, this work does not take in to account layered heterogeneity, nonlinear creep, and various loading conditions.

The compressibility of soft soil exhibits time-dependent effects, such as creep and strain rate dependency, that are typically not included in consolidation theory (Yin et al. 2002; Feng et al. 2020), and researchers have proposed methods to take these effects into account. Šuklje (1957) originally proposed the isotach model to represent strain rate-dependent soil compressibility in an effective stress-strain diagram using a set of parallel constant strain rate lines (called isotachs). Šuklje also stated that the strain rate (i.e., reflecting the change rate of void ratio) is given by the prevailing effective stress and strain. Instead of parallel constant strain rate lines, Bjerrum (1967) used a group of parallel "time lines" to express the relationship between effective stress, void ratio, and time, and also assumed that the "delayed compression" (i.e., creep) rate is given by the current void ratio and effective stress. In Bjerrum's work, no general mathematical expressions were provided and the method is only applicable for instantaneous loading conditions. Based on the concept of "time lines", Yin and Graham (1989) proposed a one-dimensional (1D) Elastic Visco-Plastic (EVP) constitutive model with one general mathematical equation for the time-dependent stress-strain relationship of clayey soils, which was further described by Yin and Graham (1994). The EVP model was subsequently incorporated into consolidation equations by Yin and Graham (1996) to simulate consolidation settlement and excess pore pressure of clay under multi-stage loading. A review article by Zdravkovic and Carter (2008) highlighted the EVP model as a pivotal step forward in the modelling of soil creep effects. Perrone (1998) developed a finite element model, called CONSOL97, for elastic visco-plastic consolidation of layered soils. Similarly, Zhu and Yin (1999b) developed a finite element model for one-dimensional EVP consolidation analysis of layered soils. More recently, an EVP consolidation analysis model was developed by Chen et al. (2021) for time-dependent settlement calculation of layered clays. The above elastic visco-plastic consolidation models are based on infinitesimal strain theory and are not applicable for large strain consolidation analysis.

In general, soil consolidation models can be divided into two categories, i.e., methods based on Hypothesis A and methods based on Hypothesis B. Hypothesis A assumes that creep effects occur only after the end of primary (EOP) consolidation stage and thus the vertical strain at the end of primary consolidation is the same regardless of layer thickness. In other words, the strain-effective stress relationship for the soil skeleton is unique (time-independent) in the primary consolidation period (without viscous compression); but becomes dependent on time (with viscous/creep compression) after primary consolidation. This is very clearly a contradiction since the time-dependence of the strain-effective stress relationship for the soil skeleton is fixed for one soil. In addition, the soil element in the zone close to the drainage boundary reaches the EOP quickly so that the "secondary" (creep) compression occurs quickly even though the average degree of consolidation is still much less than 95% to 100%. This means that according to the average degree of consolidation, the soil is still in the period of "primary" consolidation, but, soil elements close to the drainage boundary have exhibited viscous/creep compression. This is another evidence that the assumption of Hypothesis A is wrong. On the other hand, Hypothesis B assumes that viscous compression occurs during and after the primary consolidation and thus the vertical strain at the end of consolidation is larger for thicker layers due to the additional time required for the consolidation process and the resulting greater accumulation of viscous compression. Methods presented by Yin and Graham (1996), Perrone (1998), and Zhu and Yin (1999b) include a time-dependent constitutive equation in the fully coupled consolidation model and thus support Hypothesis B. These methods may be called fully coupled rigorous Hypothesis B methods to distinguish them from the recently presented simplified Hypothesis B methods (Yin and Feng 2017, Feng and Yin 2017, Chen et al. 2021).

Several researchers investigated the consolidation of various soft soils exhibiting viscous/creep behavior from physical model tests. Berre and Iversen (1972) observed that total consolidation settlements at the end of primary consolidation were dependent on the thickness of the clay, meaning that Hypothesis A underestimated soil consolidation settlements. Imai and Tang (1992) performed two sets of experiments on clay specimens using inter-connected consolidometers to effectively create the effect of different total soil thicknesses. In one set of tests, load increments were applied immediately after primary consolidation and, in the other set, loads were applied after 24 hours. Imai and Tang (1992) concluded that the incremental nominal strain-effective stress relationships from the former and later tests support Hypothesis A and Hypothesis B, respectively, and that creep compression occurs throughout the consolidation process. Degago et al. (2011) pointed out that physical model test data should be presented as absolute nominal strain vs. effective stress and, when done in this way, from the data from Imai and Tang (1992) and a few other papers support, in fact, Hypothesis B. Mesri and Choi (1987) developed the concept of a constant C_{ae}/C_c ratio (i.e., ratio of secondary compression index C_{ae} to compression index C_c) for different soil types. Mesri et al. (1995) and Mesri (2003) then combined this concept with Hypothesis A to model soil consolidation and secondary compression behavior. Using the isotache method, Leroueil (2006) indicated that the C_{ae}/C_c ratio is likely not a constant value but decreases with decreasing strain rate. Leroueil et al. (1985) found a unique relationship between effective stress, strain, and strain rate throughout the consolidation and secondary compression stages that supports Hypothesis B. Degago et al. (2011) reviewed the various isotache models and relevant experimental investigations and found that all data from measurements and numerical simulations with a time-dependent stress-strain relationship supported the validation of the rigorous Hypothesis B method.

Based on CS2 model proposed by Fox and Berles (1997) and the 1D EVP constitutive model proposed by Yin and Graham (1989; 1994), this paper presents a one-dimensional (1D) piecewise-linear model for large strain consolidation analysis of multilayered soils using an extended 1D Elastic Visco-Plastic (EVP) model, called a CS-EVP. CS-EVP can accommodate effects of large vertical strain, nonlinear creep with creep limit, variable hydraulic conductivity during the consolidation process, variable boundary conditions, and time-dependent loading due to self-weight and surcharge and/or vacuum for a layered soil system. The capabilities of CS-EVP are demonstrated through a comparison of results with the commercial software PLAXIS and with the measurements from a large-scale laboratory slurry consolidation test. Finally, CS-EVP results are compared with measurements of settlement and excess pore pressure for layered clays taken at the field loading site in Väsby, Sweden, over a 55-year period.

Model Description

Geometry

The geometry for the CS-EVP model is presented in Fig. 1. A total number of R saturated homogeneous soil layers with an initial height of H_{1o}, H_{2o}, … and H_{Ro}, respectively, are treated as idealized two-phase materials in which soil particles and pore water are assumed to be incompressible. The term "homogeneous" refers to the constitutive relationships for each soil layer and not the vertical distributions of initial void ratio and initial vertical effective stress. Fig. 1(a) presents the initial geometry prior to loading at time t = 0. Vertical coordinate z, layer coordinate m, and element coordinate j are defined as positive-upward from a fixed datum at the bottom boundary of the soil layers. The first, second, …, and R^{th} layers are uniformly subdivided into $R_{j,1}$, $R_{j,2}$, …, and $R_{j,R}$ elements, respectively, and thus the whole soil column has a total number of elements $R_{jT} = \sum_{m=1}^{R} R_{j,m}$. Elements in a given layer have unit cross-sectional area, constant initial height (e.g., L_{1o}, L_{2o}, and L_{Ro}), and a central node located at an initial elevation (e.g., $z_{2,n\text{-}1}$ for element 2,n-1). Nodes remain at the center of their respective elements and translate vertically during the consolidation process, as shown in Fig. 1(b). Top and bottom boundaries may be undrained, freely drained, or vacuum drained. For the drained cases, constant total head values, h_t and h_b, relative to the datum, are specified for the top and bottom boundaries, respectively. When different, these specified head values create the effect of an external hydraulic gradient across the layers. Both the distributions of initial void ratio and initial vertical effective stress within the layers are assigned by the user prior to the start of calculation.

Constitutive Relationships

The 1D Elastic Visco-Plastic (1D EVP) constitutive model presented by Yin and Graham (1989, 1994) is extended in this paper and implemented in the CS2 model framework originally proposed by Fox and Berles (1997). The extended 1D EVP model represents a time-dependent relationship between void ratio *e* and vertical effective stress σ'. In deriving the original 1D EVP model by Yin and Graham (1989, 1994), as shown in Fig. 2, the strain of the "instant time" line (elastic) ε^e in Eq. 1, the strain of the "reference time" line ε^r in Eq. 2, and creep strain (time-dependent) ε^{vp} in Eq. 3, are expressed as follows:

$$\varepsilon^e = \varepsilon_i^e + \kappa / V \times \ln\left(\sigma' / \sigma_i'\right) \tag{1}$$

$$\varepsilon^r = \varepsilon_o^r + \lambda / V \times \ln\left(\sigma' / \sigma_{ro}'\right) \tag{2}$$

$$\varepsilon^{vp} = \psi / V \times \ln\left[\left(t_o + t_e\right) / t_o\right] \tag{3}$$

where κ, λ and ψ refer to slopes of the "instant time" line with $\ln\left(\sigma' / \sigma_i'\right)$, the "reference time" line with $\ln\left(\sigma' / \sigma_{ro}'\right)$, and the creep line with $\ln\left[\left(t_o + t_e\right) / t_o\right]$, respectively; *V* denotes the specific volume (1+*e*); σ_i' is a unit-reference effective stress for the "instant time" line and σ_{ro}' is similar to a pre-consolidation pressure and is a stress point on the "reference time" line; ε_i^e and ε_o^r are the strains corresponding to effective stresses σ_i' and σ_{ro}', respectively; t_e refers to the equivalent time, and t_o denotes a soil parameter.

According to the "equivalent time" concept and the EVP model framework (Yin and Graham 1989; 1994), the total vertical strain at any stress state is given by:

$$\varepsilon = \varepsilon^r + \varepsilon^{vp} = \varepsilon_o^r + \lambda / V \ln\left(\sigma' / \sigma'_{ro}\right) + \psi / V \ln\left[\left(t_o + t_e\right) / t_o\right] \quad (4)$$

and the corresponding void ratio is:

$$e = e_o^r - \lambda \ln\left(\sigma' / \sigma'_{ro}\right) - \psi \ln\left[\left(t_o + t_e\right) / t_o\right] \quad (5)$$

Conversely, once the stress and strain state of the soil are known, the equivalent time t_e can be determined as

$$t_e = -t_o + t_o \exp\left[\left(e_o^r - e\right) / \psi\right]\left(\sigma' / \sigma'_{ro}\right)^{-\lambda/\psi} \quad (6)$$

Fig. 2 shows the elastic visco-plastic $e - \sigma' - t_e$ constitutive relationship. In response to the applied vertical stress increment $d\sigma'$, the decrease of void ratio *de* after a period of consolidation time *dt* is given as

$$de = de^e + de^{vp} = \frac{\kappa}{\sigma'} d\sigma' + de^{vp} \quad (7)$$

where de^e refers to the reduction of void ratio due to increase of elastic strain, and de^{vp} is the total reduction of void ratio due to creep strain.

The rate of void ratio change $\dot{e}$ is determined as

$$\dot{e} = \dot{e}^e + \dot{e}^{vp} = \frac{de}{dt} = \frac{de^e}{dt} + \frac{de^{vp}}{dt} \quad (8)$$

where $\dot{e}^e = de^e / dt$ is the elastic strain rate and $\dot{e}^{vp} = de^{vp} / dt$ is the visco-plastic strain rate. According to the "equivalent time" concept (Yin and Graham 1989; 1994), the creep rate from the reference time line is de^{vp} / dt_e. For the same strain-effective stress state point, the two visco-plastic strain rates are equal, that is, $\dot{e}^{vp} = de^{vp} / dt = de^{vp} / dt_e$. Combining Eqs. 6 and 8 gives

$$\frac{de^{vp}}{dt} = \frac{de^{vp}}{dt_e} = \frac{\psi}{t_o + t_e} = \frac{\psi}{t_o} \exp\left(\frac{e - e_o^r}{\psi}\right)\left(\frac{\sigma'}{\sigma'_{ro}}\right)^{\lambda/\psi} \quad (9)$$

and substituting Eqs. 8 and 9 into Eq. 7, the change of void ratio for a period of time *dt* can be calculated as

$$de = \frac{\kappa}{\sigma'} d\sigma' + \frac{\psi}{t_o} \exp\left(\frac{e - e_o^r}{\psi}\right)\left(\frac{\sigma'}{\sigma'_{ro}}\right)^{\lambda/\psi} dt \tag{10}$$

Eq. 10 is a general relationship of $de - d\sigma' - dt_e$ for the elastic visco-plastic model used in CS-EVP. Six soil parameters (i.e., κ, λ, ψ, σ'_{ro}, e_o^r, and t_o) are required as input values. For normally consolidated soils, e_o can be used as e_o^r. Once the decrease of void ratio de for time increment dt is known, the change of effective stress can be determined as

$$d\sigma' = \left(de - \frac{\psi}{t_o} \exp\left(\frac{e - e_o^r}{\psi}\right)\left(\frac{\sigma'}{\sigma'_{ro}}\right)^{\lambda/\psi} dt\right) \times \frac{\sigma'}{\kappa} \tag{11}$$

For constant creep parameter ψ, Eq. 3 indicates that creep strain becomes infinite for infinite time, which would overestimate long-term settlement. To overcome this limitation, Yin (1999) proposed a nonlinear creep function with limited creep strain as follows

$$\varepsilon^{vp} = \frac{(\psi_o / V)\ln\left[(t_o + t_e)/t_o\right]}{1 + \left[\psi_o / \left(V\varepsilon_L^{vp}\right)\right]\ln\left[(t_o + t_e)/t_o\right]} \tag{12}$$

where ψ_o is a constant and corresponds to the initial value of ψ in Eq. 3 at $t_e = 0$, and ε_L^{vp} denotes the limit of creep strain (Fig. 2). Then, the total vertical strain at any stress state is

$$\varepsilon = \varepsilon^r + \varepsilon^{vp} = \varepsilon_o^r + \frac{\lambda}{V}\ln\left(\frac{\sigma'}{\sigma'_{ro}}\right) + \frac{(\psi_o / V)\ln\left[(t_o + t_e)/t_o\right]}{1 + \left[\psi_o / \left(V\varepsilon_L^{vp}\right)\right]\ln\left[(t_o + t_e)/t_o\right]} \tag{13}$$

From Eq. 13, the equivalent time t_e for nonlinear creep is given by

$$t_e = -t_o + t_o \exp\left[\frac{\varepsilon - \varepsilon_r}{(\psi_o / V)\left(1 - (\varepsilon - \varepsilon_r)/\varepsilon_L^{vp}\right)}\right] \tag{14}$$

where $\varepsilon^r = \varepsilon_o^r + \lambda / V \ln\left(\sigma' / \sigma'_{ro}\right)$. Differentiating Eq. 12 with equivalent time t_e (Eq. 14) gives

$$\frac{d\varepsilon^{vp}}{dt_e} = \frac{\psi_o}{Vt_o}\left(1 + \frac{\left(\varepsilon^r - \varepsilon\right)}{\varepsilon_L^{vp}}\right)^2 \exp\left[\frac{\left(\varepsilon^r - \varepsilon\right)}{\left(1 + \left(\varepsilon^r - \varepsilon\right)/\varepsilon_L^{vp}\right)}\frac{V}{\psi_o}\right] \tag{15}$$

and the corresponding rate of void ratio change is:

$$\frac{de^{vp}}{dt_e} = \frac{\psi_o}{t_o}\left(1+\frac{e-e^r}{e_L^{vp}}\right)^2 \exp\left(\frac{e-e^r}{1+\left(e-e^r\right)/e_L^{vp}}\frac{1}{\psi_o}\right) \quad (16)$$

where $e^r = e_o^r + \lambda \ln\left(\sigma'/\sigma'_{ro}\right)$, and e_L^{vp} corresponds to ε_L^{vp} and is the void ratio at limiting creep strain as shown in Fig. 2. Similarly, $de^{vp}/dt = de^{vp}/dt_e$ based on the "equivalent time" concept, and applying Eq. 16 to Eq. 7, the change of void ratio for nonlinear creep is determined as

$$de = \frac{\kappa}{\sigma'}d\sigma' + \frac{\psi_o}{t_o}\left(1+\frac{e-e^r}{e_L^{vp}}\right)^2 \exp\left(\frac{e-e^r}{1+\left(e-e^r\right)/e_L^{vp}}\frac{1}{\psi_o}\right)dt \quad (17)$$

The relationship between the change of void ratio and the increment of effective stress with nonlinear creep is determined from Eq. 17 and expressed as

$$d\sigma' = \left(de - \frac{\psi_o}{t_o}\left(1+\frac{e-e^r}{e_L^{vp}}\right)^2 \exp\left(\frac{e-e^r}{1+\left(e-e^r\right)/e_L^{vp}}\frac{1}{\psi_o}\right)dt\right) \times \frac{\sigma'}{\kappa} \quad (18)$$

where $e^r = e_o^r + \lambda \ln\left(\sigma'/\sigma'_{ro}\right)$, and e_L^{vp} corresponds to ε_L^{vp} and is the void ratio at limiting creep strain as shown in Fig. 2.

Three parameters, t_o, e_L^{vp}, and ψ_o, are used to characterize the nonlinear creep behaviour, and these parameters can be determined through curve fitting using oedometer results (Yin 1999). The nonlinear creep equation can be expressed as $\ln\left[\left(t+t_o\right)/t_o\right]/\Delta\varepsilon = 1/\psi_o + 1/\varepsilon_L^{vp} \ln\left[\left(t+t_o\right)/t_o\right]$, where $\Delta\varepsilon$ represents the strain increase caused solely by creep, excluding any instantaneous strain, and t is the creep time corresponding to $\Delta\varepsilon$. The strain observed after the dissipation of excess pore pressure corresponds to the creep strain in oedometer tests, enabling direct determination of $\Delta\varepsilon$ and t from the oedometer test data. The selection of t_o is typically predetermined in the curve-fitting process, and the measured data of $\Delta\varepsilon$ and t are used to calculate the relationship between the normalized ratio $\ln\left[\left(t+t_o\right)/t_o\right]/\Delta\varepsilon$ and $\ln\left[\left(t+t_o\right)/t_o\right]$.

For an appropriate t_o, a straight line and fitting equation can be obtained with *x* and *y* coordinates correspond for $\ln\left[\left(t+t_o\right)/t_o\right]$ and $\ln\left[\left(t+t_o\right)/t_o\right]/\Delta\varepsilon$, respectively. Ultimately, ψ_o and ε_L^{vp} can be determined from the constant coefficient of the best fitting equation.

The hydraulic conductivity constitutive relationship for CS-EVP, as shown in Fig. 3, is defined by *Rt* pairs of corresponding vertical hydraulic conductivity *k* and void ratio *e*, e.g., $\left(\bar{e}_1,\bar{k}_1\right)$, $\left(\bar{e}_t,\bar{k}_t\right)$ and $\left(\bar{e}_{Rt},\bar{k}_{Rt}\right)$. Similar to CS2, any desired form of the hydraulic conductivity relationship can be represented (Fox and Berles 1997).

Vertical Stress

The vertical total stress σ for each element is calculated by

$$\sigma_{m,j}^{t}=\sigma'_{o,m,j}+\Delta q^{t}+\left(h_t-H^{t}\right)\gamma_w+\frac{L_{m,j}^{t}\gamma_{m,j}^{t}}{2}+\sum_{x=j+1}^{R_{j,m}}L_{m,x}^{t}\gamma_{m,x}^{t} \tag{19}$$

where γ_w refers to the unit weight of pore water; h_t is total head at the top boundary; H^t is the total height of soil layers at time *t*; $L_{m,j}^{t}$ is the thickness of element *m*, *j* at time *t*; and $\gamma_{m,j}^{t}$ is the saturated unit weight of element *m*, *j* at time *t*. Then, following the effective stress principle, the pore pressure for element *m*, *j* at time *t*, $u_{m,j}^{t}$, can be determined as

$$u_{m,j}^{t}=\sigma_{m,j}^{t}-\sigma'^{t}_{m,j} \tag{20}$$

Flow and Settlement

The equivalent vertical hydraulic conductivity between adjacent element nodes *m*, *j* and *m*, *j*+1 is computed as

$$k_{s,m,j}^{t}=\frac{\left(L_{m,j}^{t}+L_{m,j+1}^{t}\right)k_{m,j}^{t}k_{m,j+1}^{t}}{L_{m,j}^{t}k_{m,j+1}^{t}+L_{m,j+1}^{t}k_{m,j}^{t}} \tag{21}$$

where $k_{s,m,j}^{t}$ is the equivalent series hydraulic conductivity between nodes m, j and m, j+1 and $k_{m,j}^{t}$ is the hydraulic conductivity for element m, j at time t.

The relative motion of solid and fluid is considered and the flow rate $v_{rf,m,j}^{t}$ from node m, j to m, j+1 is

$$v_{rf,m,j}^{t} = -k_{s,m,j}^{t} i_{m,j}^{t} \tag{22}$$

where $i_{m,j}^{t}$ is the hydraulic gradient from node m, j to node m, j+1 $i_{m,j}^{t} = \left(h_{m,j+1}^{t} - h_{m,j}^{t}\right) / \left(z_{m,j+1}^{t} - z_{m,j}^{t}\right)$ and $h_{m,j}^{t}$ is the total hydraulic head at node m, j

$$h_{m,j}^{t} = z_{m,j}^{t} + \frac{u_{m,j}^{t}}{\gamma_w} \tag{23}$$

For the bottom boundary, the hydraulic gradient is $i_{1,o}^{t} = 0$ for impervious boundary; $i_{1,o}^{t} = \left(h_{1,1}^{t} - h_b\right) / z_{1,1}^{t}$ for freely drained boundary and $i_{1,o}^{t} = \left(h_{1,1}^{t} - \Delta p^t / \gamma_w\right) / z_{1,1}^{t}$ for vacuum drained boundary, where Δp^t is the vacuum applied at time t. Similarly, for the top boundary, the corresponding hydraulic gradients for impervious, freely drained, and vacuum drained boundaries are $i_{R_{jT}}^{t} = 0$, $i_{R_{jT}}^{t} = \left(h_t - h_{R_{jT}}^{t}\right) / \left(H^t - z_{R_{jT}}^{t}\right)$ and $i_{R_{jT}}^{t} = \left(\Delta p^t / \gamma_w - h_{R_{jT}}^{t}\right) / \left(H^t - z_{R_{jT}}^{t}\right)$, respectively. Once the flow rates are known, considering only vertical strain, the updated thickness and void ratio for element m, j at time t+Δt are determined as

$$L_{m,j}^{t+\Delta t} = L_{m,j}^{t} - (v_{rf,m,j}^{t} - v_{rf,m,j-1}^{t})\Delta t \tag{24}$$

$$e_{m,j}^{t+\Delta t} = \frac{L_{m,j}^{t+\Delta t}(1 + e_{o,m,j})}{L_{mo}} - 1 \tag{25}$$

and the change of void ratio for time increment Δt is calculated as

$$\Delta e_{m,j}^{\Delta t} = e_{m,j}^{t} - e_{m,j}^{t+\Delta t} \tag{26}$$

The value of $\Delta e_{m,j}^{\Delta t}$ from Eq. 22 is used in Eq. 11 or Eq. 18 to calculate the change of effective stress corresponding to time increment Δt. For small values of time increment, dt in Eqs. 11 and 18 is considered equal to Δt, and thus $\Delta e = de$. At time t+Δt, the total settlement of soil layers $S^{t+\Delta t}$ is calculated as

$$S^{t+\Delta t} = H_o - \sum_{m=1}^{R} \sum_{j=1}^{R_{j,m}} L_{m,j}^{t+\Delta t} \tag{27}$$

Time Increment

CS-EVP uses explicit time integration with time increment Δt calculated at each time step according to three constraints. The constraints of numerical stability and accurate time integration of discharge velocity near drainage boundaries are expressed as (Fox and Berles 1997)

$$\Delta t = \min \left\{ \frac{\alpha \gamma_w a_{v,m,j}^t \left(L_{m,j}^t \right)^2}{k_{m,j}^t \left(1 + e_{m,j}^t \right)}, \left| \frac{0.0001 L_{mo} \left(e_{o,m,j} - e_{af} \right)}{\left(1 + e_{o,m,j} \right) \left(v_{rf,m,j}^t - v_{rf,m,j-1}^t \right)} \right| \right\} \tag{28}$$

where $\alpha = 0.4$, $a_{v,m,j}^t$ refers to the coefficient of compressibility $\Delta e_{m,j}^t / \Delta \sigma_{m,j}^{\prime t}$, and e_{af} is the final void ratio with a recommended value of 0.1. This final void ratio cannot be calculated from the compressibility relationship a priori due to the time-dependency effect and must be assumed as an approximate value. Loading schedules (i.e., Δq^t and Δp^t) are considered as a third constraint to determine Δt. CS-EVP then uses the minimum Δt to advance the computation forward for all elements.

Model Validation

Comparison with PLAXIS

The performance of the CS-EVP model is demonstrated using two examples of soil consolidation and results are compared with results from the finite element software PLAXIS 2D. The initial mesh geometry of two examples for PLAXIS is shown in Fig. 3 and soil input parameters are provided in Table 1. Example 1 involves a three-layer soil column with a total initial height of 10 m and the initial heights of interior layers 1, 2, and 3 of 4 m, 4 m, and 2 m, respectively. For example 2, three single-layer soil columns with initial heights of 4 m, 8 m, and 12 m are investigated, with soil parameters from the top soil layer in example 1 used for all columns in example 2. A surcharge of 20 kPa is applied to the top of columns at time $t = 0$ and held constant thereafter. The top boundary is drained and bottom boundary undrained. Strain occurs only in the vertical direction and side friction is neglected. The PLAXIS simulation used an updated mesh and pore pressure analysis to account for large strains and the soft soil creep model (SSC) to account for time-dependent strains. The relationship between hydraulic conductivity and void ratio, which is the only available nonlinear *k*-*e* relationship in PLAXIS, is expressed as

$$k = k_o \times 10^{(e-e_o)/C_k} \tag{29}$$

where k_o is the initial hydraulic conductivity corresponding to initial void ratio e_o and C_k is the hydraulic conductivity change index. Noted that CS-EVP can accommodate essentially any desired *k*-*e* form.

The settlement versus time relationships for each layer in the soil column of example 1, as obtained from CS-EVP and PLAXIS, are shown in Fig. 4(a). At $t = 1\times10^6$ days, total settlements at the top of layers 1, 2, and 3, are 1.21 m, 2.43 m, and 3.13 m, respectively, and yield average vertical strains of 30.3%, 30.4%, and 31.3%. These strains decrease slightly with depth due to the lower initial void ratio (due to soil self-weight). The results from CS-EVP and PLAXIS are in good agreement, with slightly higher settlements calculated using CS-EVP. Corresponding values of excess pore pressure within the column are shown in Fig. 4(b). Excess pore pressures dissipate more quickly closer to the top drainage boundary as expected and again show close agreement with the PLAXIS simulation. An excess pore pressure slightly higher than the applied load is indicated in the early consolidation phase for both CS-EVP and PLAXIS simulations, especially for elevations away from the drainage boundary. This effect was first simulated in the EVP consolidation model reported by Yin et al. (1994) and results from effective stress relaxation in the soil prior to pore water drainage. In general, excess pore pressures obtained from CS-EVP are slightly higher than from PLAXIS, which is consistent with the slightly higher settlements and average vertical strains for CS-EVP in Fig. 4(a).

For the same example 1, CS-EVP is used to investigate the sensitivity of consolidation behaviour to nonlinear creep parameters. In the analysis, a controlled variable approach is used, wherein one of the nonlinear creep parameters is modified while keeping the other two parameters constant. For the nonlinear creep simulations, values of creep parameter ψ_o are set equal to ψ (Table 1). Settlement relationships at the top of layer 1 (z_o = 4 m) and top of layer 3 (z_o = 10 m) using various values of e_L^{vp}, t_o, and ψ_o, are shown in Fig. 5. Constant creep and nonlinear creep settlements agree well at early time but diverge later during the consolidation stage, with the divergence increasing for smaller e_L^{vp}. Similar patterns are observed in numerical simulations with different t_o and ψ_o. A smaller long-term settlement is observed for a larger t_o and a smaller ψ_o. This occurs because the nonlinear creep strain decreases gradually with increasing elapsed time. The parameters e_L^{vp} and ψ_o have a more significant influence on long-term consolidation settlements, compared to parameter t_o. Currently, PLAXIS is limited to a constant creep.

CS-EVP and PLAXIS results for the three columns of example 2 are presented in Fig. 6. Settlement relationships for the top boundaries of the columns are shown in Fig. 6(a) and indicate larger settlement for larger initial column height. Corresponding plots for excess pore pressure at the bottom (impervious) boundary are shown in Fig. 6(b) and indicate faster dissipation for the shorter columns due to the reduced drainage path. Plots of average vertical strain (i.e., settlement/H_o) are shown in Fig. 6(c) and indicate that the strain associated with the end of primary (EOP) consolidation increases with initial column height. This finding is consistent with Hypothesis B and results from accumulating time-dependent visco-plastic strain within the soil skeleton during the consolidation process. The three plots in Fig. 6 also indicate close agreement between CS-EVP and PLAXIS results.

Comparison with Laboratory Slurry Consolidation Test

A large-scale laboratory consolidation test of a high-water-content soil slurry was performed to further demonstrate the capability of CS-EVP. Hong Kong marine deposits obtained from a dredging project in Tuen Mun, Hong Kong were utilized for the test. The soil deposits had a natural water content of approximately 90% (i.e., 1.5 times the liquid limit) and are classified as

CH, fat clay according to the Unified Soil Classification System (ASTM D2487-17). Soil properties are provided in Table 2.

The testing apparatus, shown in Fig. 7, consisted of eight cylindrical plexiglass segments, each with an internal diameter of 170 mm, wall thickness of 10 mm, and height of 100 mm, giving a total cylinder height of 800 mm. A valve was installed at the mid-height of each segment to permit the collection of small slurry samples during consolidation for soil water content determination. Settlement at the top of the soil column was measured throughout the test. Consolidation occurred from soil self-weight and vacuum applied at the base of the specimen using a prefabricated horizontal drain (PHD), which created a one-dimensional consolidation condition. The PHD was connected to an air-water separator and vacuum pump. The column was freely drained at the top boundary with a plastic film placed over the top to reduce desiccation.

The initial water content of the soil slurry was 265%, which is approximately 4 times the liquid limit. The well-mixed slurry was poured into the test apparatus to an initial height of 800 mm at time $t = 0$. The initial void ratio profile, as determined from measured water contents, is shown in Fig. 8. The top value is slightly higher than at the bottom value due to the rapid sedimentation of larger particles. The slurry specimen was allowed to consolidate under self-weight for 4 days with a no flow condition at the bottom boundary. Over the next 33 days, vacuum was applied to the bottom boundary in three increments of -20 kPa, -40 kPa and -80 kPa, as shown in Fig. 9.

CS-EVP simulations were conducted for the same laboratory consolidation test with H_o = 0.8 m, $G_s = 2.63$, $\kappa = 0.0005$, $\lambda = 0.711$, $\psi = 0.012$, and $t_o = 1440$ min based on additional results from an oedometer test. A uniform initial void ratio e_o = 6.96 was specified based on the average of measured water contents (Fig. 8). Initial values of vertical effective stress and hydraulic conductivity for the slurry were back-calculated using oedometer test results, giving $\sigma'_o = \sigma'_{ro}$ = 0.016 kPa and k_o = 1.7 × 10^{-6} m/s. Three values of C_k = 1.68, 1.78, and 1.88, which are within the range of back-calculated values shown in Table 2, were selected for simulations. The top boundary was freely drained during the entire simulation period and the bottom boundary was impermeable during the self-weight consolidation stage and pore pressure-controlled after the application of vacuum. A total of 30 elements were used for each soil layer in the CS-EVP simulations.

Fig. 10 presents settlement versus time relationships obtained from the slurry consolidation test and CS-EVP simulations for three values of C_k. Total settlements after 4 days of self-weight consolidation and 33 days of self-weight and vacuum consolidation are 0.1 m and 0.45 m, respectively, corresponding to average vertical strains of 12.5% and 56.3%. The plot indicates that the rate of consolidation significantly increases after the application of vacuum to the bottom boundary. The settlement relationship obtained from CS-EVP with C_k = 1.78 is in close agreement with the experimental measurements throughout the test. Corresponding relationships obtained using C_k = 1.68 and 1.88 indicate slower and faster consolidation rates during the vacuum consolidation stage, respectively. Final settlement increases with increasing C_k because greater creep occurs with the overall larger effective stress in the slurry column during the testing period. During the self-weight consolidation stage, simulated consolidation rates show little divergence, and are slightly slower than the observed rate due to the assumption of constant C_k.

Profiles of soil void ratio are presented in Fig. 11 along with simulated values from CS-EVP with three values of C_k. During the self-weight consolidation stage (i.e., $t = 2$ days and $t = 4$ days), void ratios are relatively uniform with slightly lower values near the top. The void ratios estimated by CS-EVP with different values of C_k are highly consistent and exhibit higher in the top section and slightly lower in the bottom section during this stage, compared to the measured data. After the application of vacuum starting at $t = 4$ days, void ratios near the bottom boundary begin to decrease rapidly and, over time, produce a strong void ratio gradient across the column. Simulations of CS-EVP with higher C_k results in slightly smaller estimated void ratios in the soil profiles, corresponding to larger simulated settlements. There are potentially three reasons for the difference between the measured and estimated void ratios: (a) inconsistencies between the assumed initial void ratio used in simulations and the actual void ratio profile; (b) potential measurement errors in the water content data used to calculate the void ratio, as well as variations in G_s within the soil profile; (c) the constant values of C_k and λ may not accurately capture the significant variations in void ratio during the large-strain consolidation process. Corresponding profiles from CS-EVP are generally in close agreement with the experimental measurements, especially for the latter stages of the test. The overall good agreements between measured and simulated results in Figs. 10 and 11 indicate that CS-EVP captured important results of this large-strain slurry consolidation test, including the effects of soil self-weight, creep, and variable compressibility and hydraulic conductivity.

Field Case Study

A second analysis was performed using CS-EVP for the field embankment test site in Väsby, Sweden. Well-instrumented field consolidation tests were conducted by the Swedish Geotechnical Institute (SGI) for site selection of a new airport. Three test embankments were constructed at the Väsby site from 1946 to 1948, with settlements and pore pressures measured thereafter for several decades. The long-term behavior of one of the test embankments, constructed without vertical drains in October 1947, is the focus of this case study. The subsurface consists of a series of thick clay layers, including at least four types of soft clay, with high water content and compressibility. A thin layer of medium grey sand lies below the clay layers and provides drainage at the bottom, thus yielding a double drained system for the site.

The gravel test embankment was constructed with a height of 2.5 m, bottom dimensions of 30 m × 30 m, 1V:1.5H side slopes, and an average unit weight of 16.2 kN/m^3. Consolidation at the center of embankment was considered essentially one-dimensional due to the large dimensions of the fill. The embankment was constructed over a 25-day period and thus provided a ramp-load surcharge with a final total vertical stress of 40.6 kPa, as shown in Fig. 12.

According to the site investigation data, the compressible soil profile had a total depth of 14 m under the fill and consisted of green organic clay, dark grey organic clay, black organic clay, dark grey organic clay, dark grey clay, grey clay, and grey varved clay in sequence from top to bottom. The natural water content of the clay layers was approximately equal to the liquid limit (70%-130%) and gradually decreased from top to bottom. For the CS-EVP analysis, the soil profile was divided into 15 layers with parameters obtained from previous studies (Chang 1981;

Larsson and Mattsson 2003; Le 2015; Chen et al. 2021), as indicated in Table 3. Unfortunately, the oedometer test results were not provided, making it impossible to determine the nonlinear creep parameters (i.e., t_o, ψ_o, and e_L^{vp}) from the available data. Consequently, three sets of nonlinear creep parameters were assumed for the numerical analysis. In the case of a specific soft soil, it has been observed that the values of e_L^{vp} and ψ_o decrease as the t_o increases (Yin and Zhu 2020). This factor was also accounted for during the parameter assumptions, with t_o values of 60 min, 120 min, and 720 min being assumed, corresponding to ψ_o values of 0.082λ, 0.072λ, 0.062λ, and corresponding e_L^{vp} values of 0.32(1+e_o), 0.30(1+e_o), and 0.28(1+e_o). Typically, t_o is chosen at a time point following the end of primary (EOP) consolidation. The ψ_o values were determined based on the commonly used ratio of the coefficient of secondary compression to the compression index (Mesri and Godlewski 1977). Additionally, a simulation was also conducted without considering creep using the elastic-plastic constitutive equation and the parameters provided in Table 3.

Long-term consolidation of the clay layers was monitored using settlement plates at the ground surface (elevation z_o = 14 m), screw-type settlement markers installed at elevation z_o = 11.5 m, 9 m, and 6.5 m, and piezometers installed at various depths. Measured time-settlement relationships from the field test are compared with CS-EVP simulations in Fig. 13. After 20,000 days, settlements of 2.02 m, 1.72 m, 1.39 m, and 0.94 m were measured at z_o = 14 m, 11.5 m, 9 m, and 6.5 m, respectively, and yield relatively consistent values of average vertical strain equal to 14.4%, 15.0%, 15.4%, and 14.5%. The field data also indicate that settlement was continuing at t = 20,000 days for each elevation. Simulated settlement relationships obtained using CS-EVP with t_o =120 min, ψ_o= 0.072λ, and e_L^{vp} =0.30(1+e_o) are in closer agreement on each plot. The simulations with t_o =60 min and 720 min resulted in slight overestimation and underestimation of the long-term settlement, respectively. Simulation that did not account for creep substantially underestimated the long-term settlements, providing evidence of the importance of considering creep in long-term consolidation analysis of soft soil layers.

Larsson and Mattsson (2003) reported that the original piezometers became unreliable and new piezometers were installed in 1968. Subsequent pore pressure measurements were also obtained in 1979 and 2002. Measured and simulated excess pore pressure profiles are compared in Fig. 14 and show maximum excess pore pressures of 30 kPa, 22 kPa and 13 kPa, after 21, 32, and 55 years, respectively. The simulated excess pore pressure profiles with t_o =120 min again show closer agreement with field measurements. Simulations conducted with different creep parameters exhibit a variation of around 10 kPa (1/4 of the surcharge load) in the maximum excess pore pressure, indicating a high sensitivity of excess pore pressure dissipation to nonlinear creep parameters. Smaller value of t_o , corresponding to larger e_L^{vp} and ψ_o , results in a reduced dissipation rate of simulated excess pore pressure. This phenomenon can be attributed to the larger simulated settlements associated with smaller t_o , which in turn leads to smaller simulated void ratios and consequently smaller hydraulic conductivity. Simulated excess pore pressures without considering creep dissipate at a noticeably faster rate compared to the measured data, further highlighting the importance of considering creep.

Conclusions

This paper presents a one-dimensional finite strain consolidation model for layered soft soils, called CS-EVP, that combines the elastic visco-plastic (EVP) constitutive model with a creep limit and the piecewise-linear CS2 method. The following conclusions are drawn:

(1) The CS-EVP accounts model for vertical strain, soil self-weight, nonlinear hydraulic conductivity, variable drainage boundary conditions, and multiple soil layers. The EVP constitutive model for the time-dependent compression of the soil skeleton considers nonlinear creep with a limit creep strain and is based on the equivalent time concept (Yin and Graham 1989, 1994).

(2) The performance of the CS-EVP model was validated through a comparison of results from a fully coupled finite element model (PLAXIS) for consolidation of single-layer and multilayer 1D soil columns. Settlement relationships and excess pore pressure profiles obtained from the two models are in close agreement. Both models support Hypothesis B and indicate that time-dependent compressibility (creep) effects have a significant influence on both short- and long-term settlements, especially for thicker soil layers due to the longer consolidation time. Long-term settlement decreases with a smaller specified value of limit creep void ratio.

(3) Results from the CS-EVP model also are compared with experimental measurements from a large-scale laboratory slurry consolidation test, involving large strain, soil self-weight, and variable drainage and boundary conditions, including applied vacuum. After 37 days of self-weight and vacuum consolidation, the thickness of the slurry decreased from 800 mm to 350

mm, yielding an average vertical strain of 56%. Settlements and void ratio profiles obtained from CS-EVP are in close agreement with laboratory measurements.

(4) The CS-EVP model was used to simulate the long-term settlement behaviour an embankment constructed at the field test site in Väsby, Sweden, in 1947. Simulated settlements at different depths and excess pore pressure profiles obtained using CS-EVP are in close agreement with field measurements over a 55-year period.

Data Availability Statement

Some or all data, models, or code that support the findings of this study are available from the corresponding author upon reasonable request.

Acknowledgements

This research was supported by the Research Grants Council of Hong Kong Special Administrative Region Government of China (Grant No.: R5037-18F, 15209119, 15210322, 15231122). The authors also acknowledge the financial support from grants (CD7A and CD82) from the Research Institute for Land and Space of Hong Kong Polytechnic University, and grants and financial support (BD8U, W23L, ZDBS) from The Hong Kong Polytechnic University. This financial support is gratefully acknowledged.

Reference

ASTM. 2017. *Standard practice for classification of soils for engineering purposes (Unified Soil Classification System)*. ASTM D2487-17, West Conshohocken, PA: ASTM International.

Berre, T., and Iversen, K. 1972. "Oedometer test with different specimen heights on a clay exhibiting large secondary compression." *Géotechnique*, 22(1), 53-70.

Bjerrum, L. 1967. "Engineering geology of Norwegian normally-consolidated marine clays as related to settlements of buildings." *Géotechnique*, 17(2), 83-118.

Borja, R. I., and Alarcón, E. 1995. "A mathematical framework for finite strain elastoplastic consolidation Part 1: Balance laws, variational formulation, and linearization." *Computer Methods in Applied Mechanics and Engineering*, 122(1-2), 145-171.

Borja, R. I., Tamagnini, C., and Alarcón, E. 1998. "Elastoplastic consolidation at finite strain part 2: finite element implementation and numerical examples." *Computer Methods in Applied Mechanics and Engineering*, 159(1-2), 103-122.

Cargill, K. W. 1984. "Prediction of consolidation of very soft soil." *Journal of Geotechnical Engineering*, 110(6), 775-795.

Carter, J. P., Booker, J. R., and Small, J. C. 1979. "The analysis of finite elasto-plastic consolidation." *International Journal for Numerical and Analytical Methods in Geomechanics*, 3(2), 107-129.

Chang, Y. C. E., 1981. *Long term consolidation beneath the test fills at Väsby*, Sweden.

Chen, R. P., Zhou, W. H., Wang, H. Z., and Chen, Y. M. 2005. "One-dimensional nonlinear consolidation of multi-layered soil by differential quadrature method." *Computers and Geotechnics*, 32(5), 358-369.

Chen, Z. J., Feng, W. Q., and Yin, J. H. 2021. "A new simplified method for calculating short-term and long-term consolidation settlements of multi-layered soils considering creep limit." *Computers and Geotechnics*, 138, 104324.

Chu, J., Bo, M. W., and Arulrajah, A. 2009. "Soil improvement works for an offshore land reclamation." *Proceedings of the Institution of Civil Engineers-Geotechnical Engineering*, 162(1), 21-32.

Degago, S. A., Grimstad, G., Jostad, H. P., Nordal, S., and Olsson, M. 2011. "Use and misuse of the isotache concept with respect to creep hypotheses A and B." *Géotechnique*, 61(10), 897-908.

Feng, W. Q., and Yin, J. H. 2017. "A New Simplified Hypothesis B Method for Calculating Consolidation Settlements of Double Soil Layers Exhibiting Creep." *International Journal for Numerical and Analytical Methods in Geomechanics*, 41, 899-917.

Feng, W. Q., Yin, J. H., Chen, W. B., Tan, D. Y., and Wu, P. C. 2020. "A new simplified method for calculating consolidation settlement of multi-layer soft soils with creep under multi-stage ramp loading." *Engineering Geology*, 264, 105322.

Feng, W. Q., Zheng, X. C., Yin, J. H., Chen, W. B., and Tan, D. Y. 2021. "Case study on long-term ground settlement of reclamation project on clay deposits in Nansha of China." *Marine Georesources & Geotechnology*, 39(3), 372-387.

Fox, P. J. 2000. "CS4: A large strain consolidation model for accreting soil layers," *Geotechnics of High Water Content Materials*, STP 1374, T. B. Edil and P. J. Fox, eds., ASTM International, West Conshohocken, Pennsylvania, 29-47.

Fox, P. J. 2007. "Coupled large strain consolidation and solute transport. I: Model development." *Journal of Geotechnical and Geoenvironmental Engineering*, 133(1), 3-15.

Fox, P. J., and Berles, J. D. 1997. "CS2: a piecewise-linear model for large strain consolidation." *International Journal for Numerical and Analytical Methods in Geomechanics*, 21(7), 453-475.

Fox, P. J., and Lee, J. 2008. "Model for consolidation-induced solute transport with nonlinear and nonequilibrium sorption." *International Journal of Geomechanics*, 8(3), 188-198.

Fox, P. J., and Pu, H. F. 2012. "Enhanced CS2 model for large strain consolidation." *International Journal of Geomechanics*, 12(5), 574-583.

Fox, P. J., Di Nicola, M., and Quigley, D. W. 2003. "Piecewise-linear model for large strain radial consolidation." *Journal of Geotechnical and Geoenvironmental Engineering*, 129(10), 940-950.

Fox, P. J., Lee, J., and Qiu, T. 2005. "Model for large strain consolidation by centrifuge." *International Journal of Geomechanics*, 5(4), 267-275.

Fox, P. J., Pu, H. F., and Berles, J. D. 2014. "CS3: Large strain consolidation model for layered soils." *Journal of Geotechnical and Geoenvironmental Engineering*, 140(8), 04014041.

Gheisari, N., Qi, S., and Simms, P. 2021. “Consolidation-creep-structuration analysis of flocculated fluid fine tailings deposits in a pilot study.” In: *GeoNiagara*, Canada.

Gheisari, N., Simms, P., Qi, S., Murphy, F., Gjerapic, G., and Znidarcic, D. 2022. “Consolidation-creep modelling in oil sands tailings deposits.” *International Soil Sands Tailings Conference*, Canada.

Gibson, R. E., England, G. L., and Hussey, M. J. L. 1967. “The theory of one-dimensional consolidation of saturated clays: I. finite non-linear consolidation of thin homogeneous layers.” *Géotechnique*, 17(3), 261-273.

Gibson, R. E., Scguffnabm, R. L., and Cargill, K. W. 1981. “The theory of one-dimensional consolidation of saturated clays. II. Finite nonlinear consolidation of thick homogeneous layers.” *Canadian Geotechnical Journal*, 18(2), 280-293.

Hazzard, J., Yacoub, T., and Curran, J. 2008. “Consolidation in multi-layered soils: a hybrid computation scheme.” *In Proc., GéoEdmonton2008: 61st Canadian Geotechnical Conf* (pp. 182-189).

Imai, G., and Tang, Y. 1992. “A constitutive equation of one-dimensional consolidation derived from inter-connected tests.” *Soils and Foundations*, 32(2), 83-96.

Kim, H. J., and Mission, J. L. 2011. “Numerical analysis of one-dimensional consolidation in layered clay using interface boundary relations in terms of infinitesimal strain.” *International Journal of Geomechanics*, 11(1), 72-77.

Larsson, R., and Mattsson, H. 2003. “Settlements and shear strength increase below embankments-long-term observations and measurement of shear strength increase by seismic cross-hole tomography.” *Swedish Geotechnical Institute Report*, 1-98.

Le, T. M. 2015. “Analysing consolidation data to optimise elastic visco-plastic model parameters for soft clay.” (Doctoral dissertation).

Lee, K. and Sills, G. C. 1981. “The consolidation of a soil stratum, including self-weight effects and large strains.” *International Journal for Numerical and Analytical Methods in Geomechanics*, 5, 405-428.

Lee, P. K. K., Xie, K. H., and Cheung, Y. K. 1992. “A study on one-dimensional consolidation of layered systems.” *International Journal for Numerical and Analytical Methods in Geomechanics*, 16(11), 815-831.

Leroueil, S. 2006. “The isotache approach-Where are we 50 years after its development by Professor Šuklje?” In *Proceedings of the XIII Danube-European Conference on Geotechnical Engineering,* Ljubljana, Slovenia, 55-88.

Leroueil, S., Kabbaj, M., Tavenas, F., and Bouchard, R. 1985. “Stress–strain–strain rate relation for the compressibility of sensitive natural clays.” *Géotechnique*, 35(2), 159-180.

Mesri, G. 2003. “Primary compression and secondary compression.” *Soil Behavior and Soft Ground Construction*, J. T. Germaine, T. C. Sheehan, and R. V. Whitman, eds., ASCE, Reston, Va., 122–166.

Mesri, G., and Castro, A. 1987. “$C\alpha/Cc$ concept and K_0 during secondary compression.” *Journal of Geotechnical Engineering*, 113(3), 230-247.

Mesri, G., and Godlewski, P. M. 1977. “Time-and stress-compressibility interrelationship.” *Journal of the Geotechnical Engineering Division*, 103(5), 417-430.

Mesri, G., Feng, T. W., and Shahien, M. 1995. “Compressibility parameters during primary consolidation.” *Proc., Int. Symp. on Compression and Consolidation of Clayey Soils*, A.A. Balkema, Rotterdam, Netherlands, 201–217

Perrone, V. J. 1998. “One dimensional computer analysis of simultaneous consolidation and creep of clay” (Doctoral dissertation, Virginia Polytechnic Institute and State University).

Pu, H. F., Fox, P. J., and Liu, Y. 2013. “Model for large strain consolidation under constant rate of strain.” *International Journal for Numerical and Analytical Methods in Geomechanics*, 37(11), 1574-1590.

Pu, H., and Fox, P. J. 2015. “Model for coupled large strain consolidation and solute transport in layered soils.” *International Journal of Geomechanics*, 16(2), 04015064.

Qi, S., Simms, P., and Vanapalli, S. 2017. “Piecewise-linear formulation of coupled large-strain consolidation and unsaturated flow. I: Model development and implementation.” *Journal of Geotechnical and Geoenvironmental Engineering*, 143(7), 04017018.

Qi, S., Simms, P., Daliri, F., and Vanapalli, S. 2020. "Coupling elasto-plastic behaviour of unsaturated soils with piecewise linear large-strain consolidation." *Géotechnique*, 70(6), 518-537.

Schiffman, R. L., and Stein, J. R. 1970. "One-dimensional consolidation of layered systems." *Journal of the Soil Mechanics and Foundations Division*, 96(4), 1499-1504.

Shen, S. L., Chai, J. C., Hong, Z. S., and Cai, F. X. 2005. "Analysis of field performance of embankments on soft clay deposit with and without PVD-improvement." *Geotextiles and Geomembranes*, 23(6), 463-485.

Šuklje, L. 1957. "The analysis of the consolidation process by the isotache method." *Proc., 4th Int. Conf. on Soil Mechanics and Foundation Engineering*, Vol. 1, Butterworths, London, 200-206.

Terzaghi, K. 1925. "Erdbaumechanik auf Bodenphishkalischer Grundlage." Wien: Franz Deuticken.

Townsend, F.C. and McVay, M.C. 1990. "SOA: large strain consolidation predictions." *Journal of Geotechnical Engineering*, 116(2), 222-243.

Xie, K. H., and Leo, C. J. 2004. "Analytical solutions of one-dimensional large strain consolidation of saturated and homogeneous clays." *Computers and Geotechnics*, 31(4), 301-314.

Xie, K. H., Xie, X. Y., and Jiang, W. 2002. "A study on one-dimensional nonlinear consolidation of double-layered soil." *Computers and Geotechnics*, 29(2), 151-168.

Yin, J. H. 1999. "Non-linear creep of soils in oedometer tests." *Géotechnique*, 49(5), 699-707.

Yin, J. H., and Feng, W. Q. 2017. "A New Simplified Method and Its Verification for Calculation of Consolidation Settlement of a Clayey Soil with Creep." *Canadian Geotechnical Journal*, 54(3), 333-347.

Yin, J. H., and Graham, J. 1989. "Viscous–elastic–plastic modelling of one-dimensional time-dependent behaviour of clays." *Canadian Geotechnical Journal*, 26(2), 199-209.

Yin, J. H., and Graham, J. 1994. “Equivalent times and one-dimensional elastic viscoplastic modelling of time-dependent stress–strain behaviour of clays.” *Canadian Geotechnical Journal*, 31(1), 42-52.

Yin, J. H., and Graham, J. 1996. “Elastic visco-plastic modelling of one-dimensional consolidation.” *Géotechnique*, 46(3), 515-527.

Yin, J. H., and Zhu, G. 2020. “Consolidation analyses of soils.” *CRC Press*, Florida.

Yin, J. H., Graham, J., Clark, J. I., and Gao, L. 1994. “Modelling unanticipated pore-water pressures in soft clays.” *Canadian Geotechnical Journal*, 31(5), 773-778.

Yin, J. H., Zhu, J. G., and Graham, J. 2002. “A new elastic viscoplastic model for time-dependent behaviour of normally and overconsolidated clays: theory and verification.” *Canadian Geotechnical Journal*, 39(1), 157-173.

Yong, R. N., Siu, S. K. and Sheeran, D. E. 1983. “On the stability and settling of suspended solids in settling ponds. Part I. Piece-wise linear consolidation analysis of settlement layer.” *Canadian Geotechnical Journal*, 20(4), 817-826.

Zdravkovic, L., and Carter, J. 2008. “Contributions to Géotechnique 1948–2008: Constitutive and numerical modelling.” *Géotechnique*, 58(5), 405-412.

Zhao, Y., and Borja, R. I. 2020. “A continuum framework for coupled solid deformation–fluid flow through anisotropic elastoplastic porous media.” *Computer Methods in Applied Mechanics and Engineering*, 369, 113225.

Zhou, Y., Deng, A., and Wang, C. 2013. “Finite difference model for one-dimensional electro-osmotic consolidation.” *Computers and Geotechnics*, 54, 152-165.

Zhu, G. F., and Yin, J. H. 1999a. “Consolidation of double soil layers under depth-dependent ramp load.” *Géotechnique*, 49(3), 415-421.

Zhu, G. F., and Yin, J. H. 1999b. “Finite element analysis of consolidation of layered clay soils using an elastic visco-plastic model.” *International Journal for Numerical and Analytical Methods in Geomechanics*, 23(4), 355-374.

Notation

a_v	coefficient of compressibility
C_c	compression index
$C_{\alpha e}$	secondary compression index in void ratio
C_k	index of change in hydraulic conductivity
e	void ratio
e_L^{vp}	limit value of creep void ratio
e_{af}	assumed final void ratio for determining of time increment
G_s	specific gravity of solids
h	total water head
h_t	total water head at top boundary
h_b	total water head at bottom boundary
H_{mo}	initial height of the m^{th} soil layer
H	height of soil layer
i	hydraulic gradient
I_p	plasticity index
j	coordinate of element
k	coefficient of permeability
k_s	equivalent coefficient of permeability
L_{mo}	initial thickness of element for the m^{th} soil layer
L	thickness of element
R	number of soil layers

$R_{j,m}$	number of elements for the m^{th} soil layer
R_{jT}	number of elements for all layers
S	settlement
t	time
t_e	equivalent time
t_o	parameter for choice of reference time line
u	pore pressure
V	specific volume
v_{rf}	discharge velocity of fluid relative to solid phase
w_p	plastic limit
z	vertical coordinate
Δp	change in vacuum
Δq	change in incremental load
$\Delta t, dt$	time increment
$\Delta \varepsilon, d\varepsilon$	strain increment
$\Delta e, de$	change in void ratio
$\Delta \sigma', d\sigma'$	change in effective stress
γ	saturated unit weight
γ_w	unit weight of pore water
σ	total stress
σ'_o	initial effective stress

σ' effective stress

σ_i' unit effective stress

σ_{ro}' parameter similar to pre-consolidation pressure

ε_i^e strain at $\sigma' = \sigma_i'$

ε_o^r strain at $\sigma' = \sigma_{ro}'$

κ the slope of instant time line with $\ln\left(\sigma' / \sigma_i'\right)$

λ the slope of a reference time line with $\ln\left(\sigma' / \sigma_{ro}'\right)$

ψ the slope of a creep line with $\ln\left[\left(t_o + t_e\right) / t_o\right]$

ψ_o the slope of a creep line with $\ln\left[\left(t_o + t_e\right) / t_o\right]$ for nonlinear creep at $t = 0$

ε^e instant strain

ε^r stress-dependent plastic strain

ε^{vp} creep strain

ε_L^{vp} limit value of creep strain

Superscripts

t time

Subscripts

m, j jth element of mth layer

List of Figures

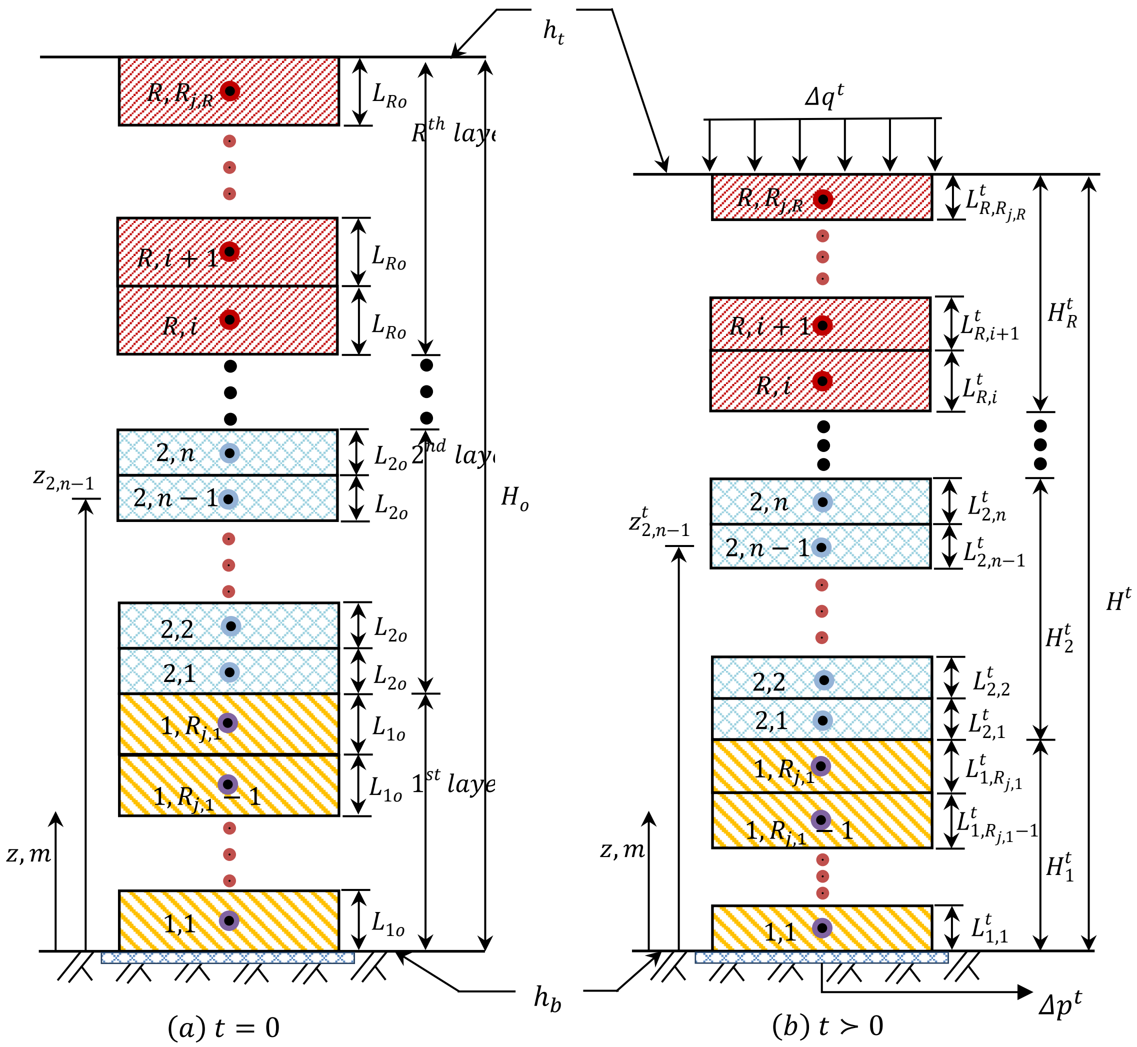

Fig. 1. CS-EVP geometry for: (a) initial condition and (b) configuration after start of consolidation

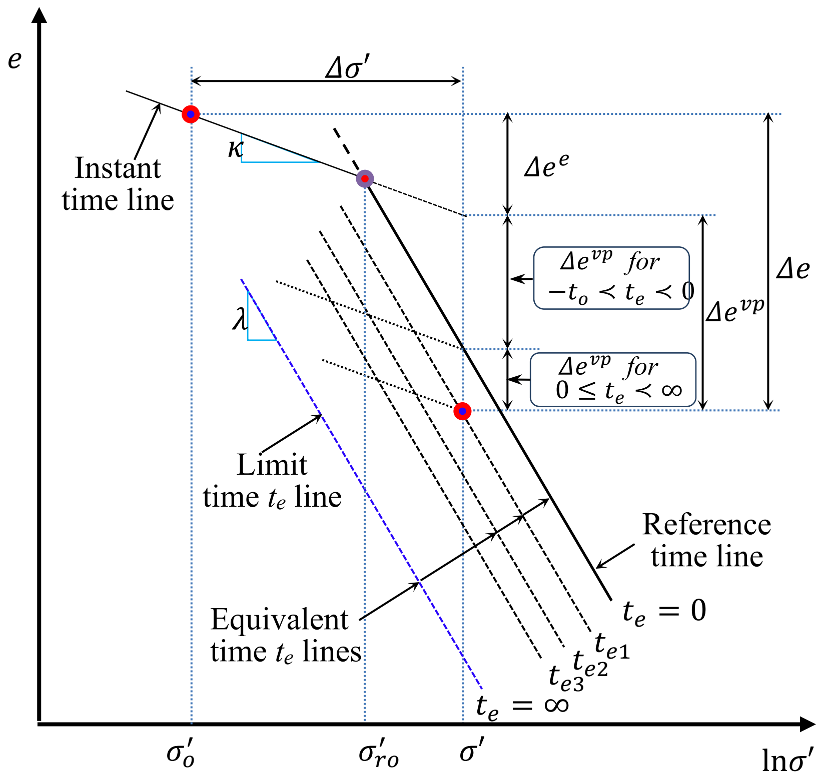

(a)

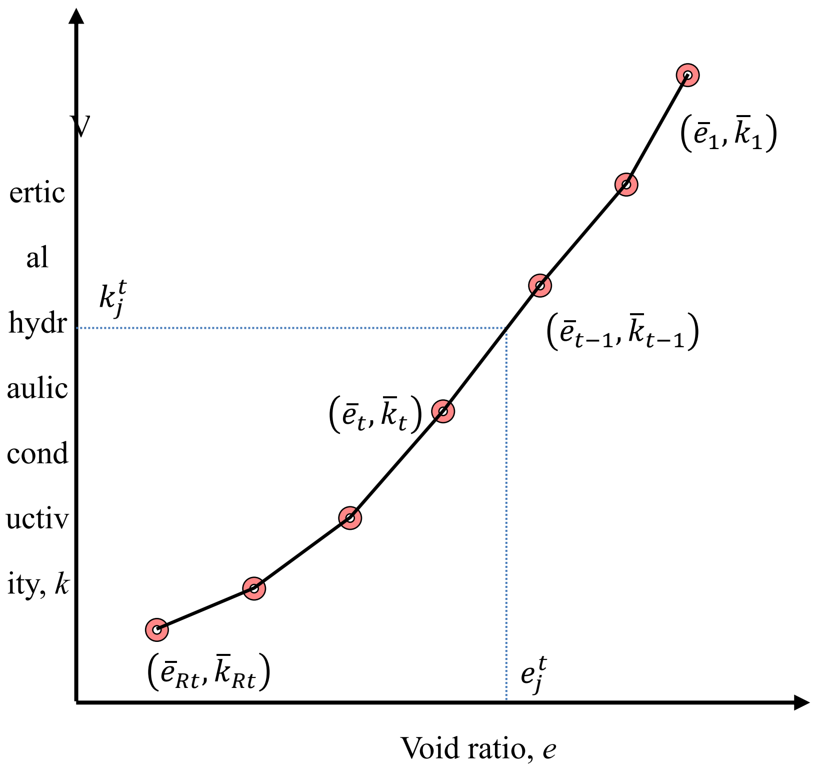

(b)

Fig. 2. Soil constitutive relationships for: (a) elastic visco-plastic compressibility, and (b) hydraulic conductivity

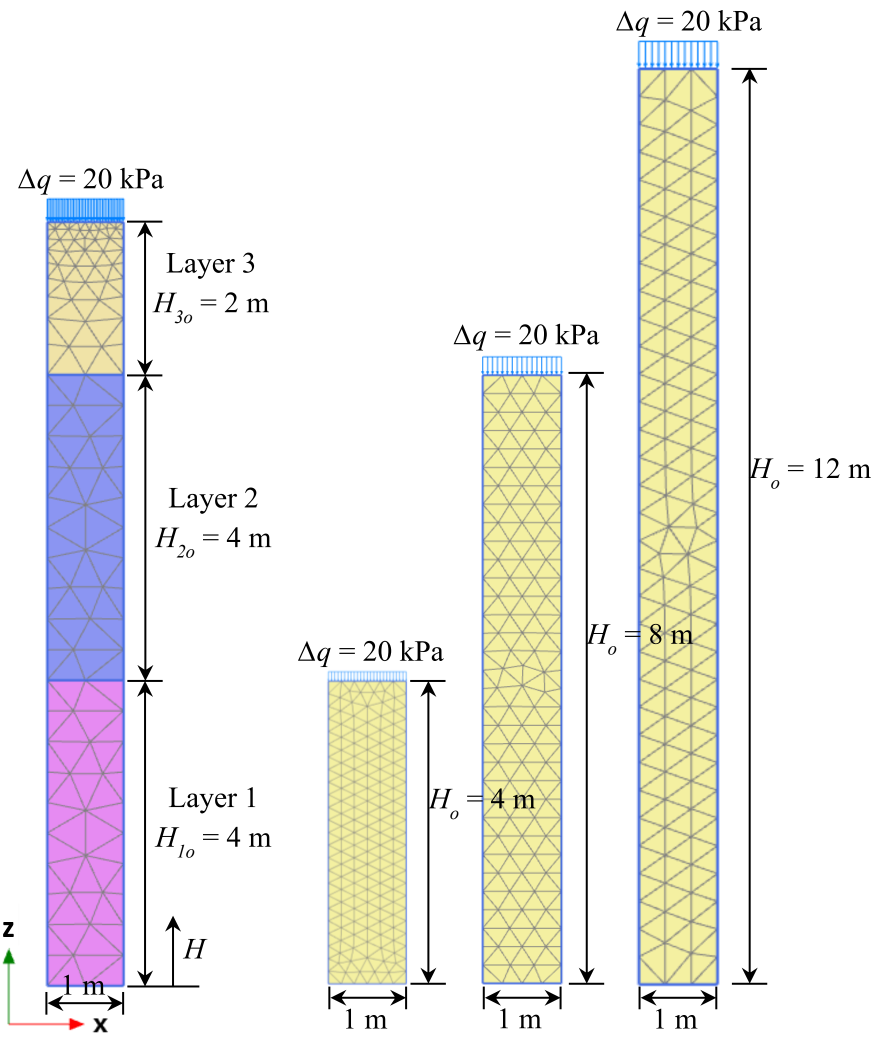

Fig. 3. Initial mesh for PLAXIS simulation of consolidation of a three-layer soil column and single-layer soil columns with different initial heights

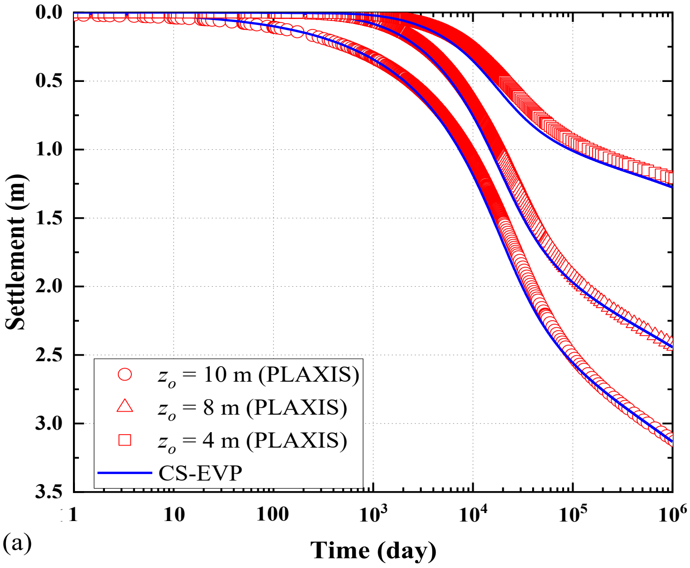

(a)

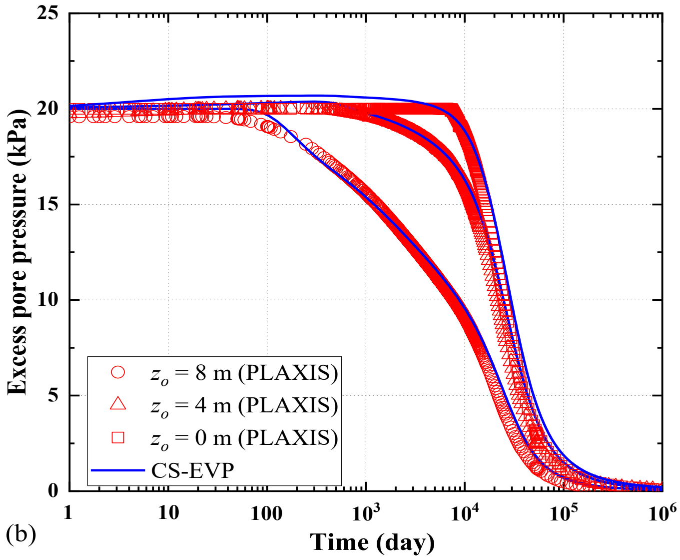

(b)

Fig. 4. Comparison of CS-EVP and PLAXIS simulation results for consolidation of a three-layer soil column: (a) settlement and (b) excess pore pressure

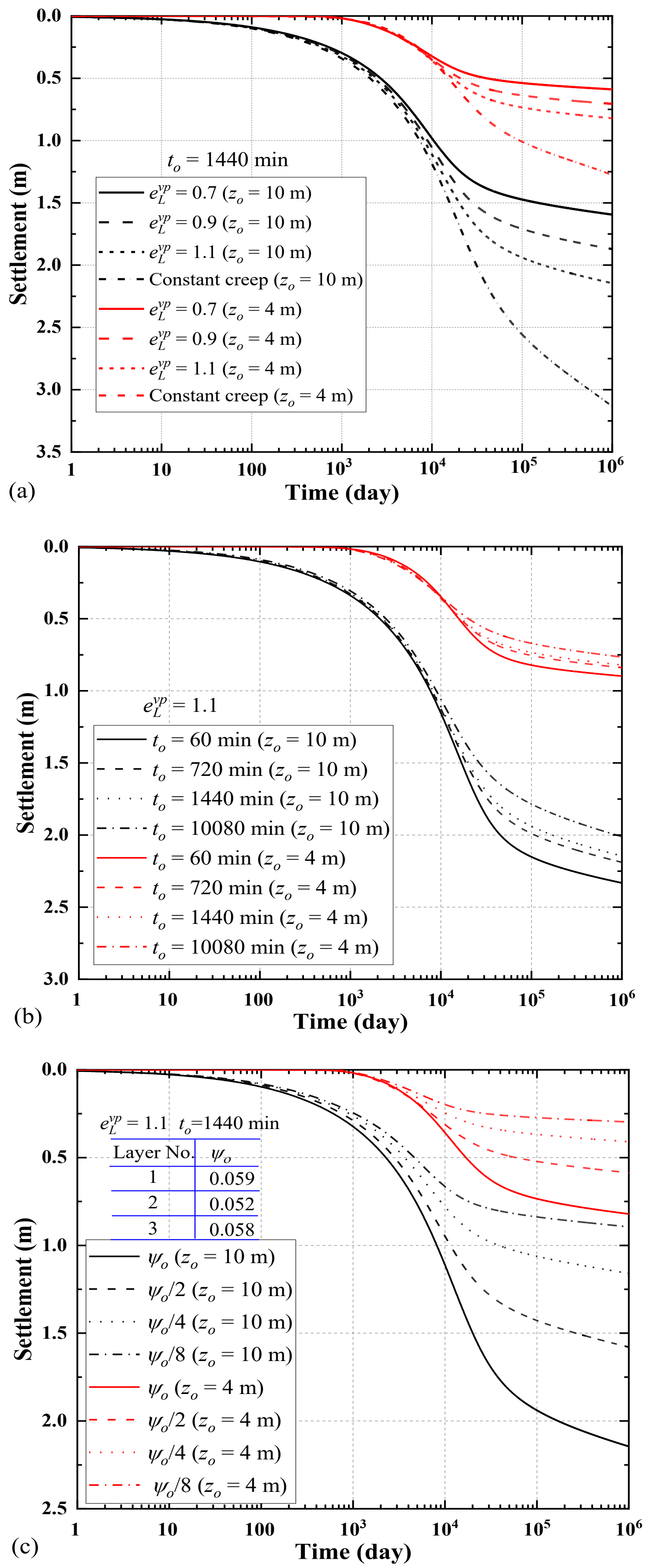

Fig. 5. Parameter-sensitive analysis of CS-EVP simulations with nonlinear creep: (a) e_L^{vp}, (b) t_o, and (c) ψ_o

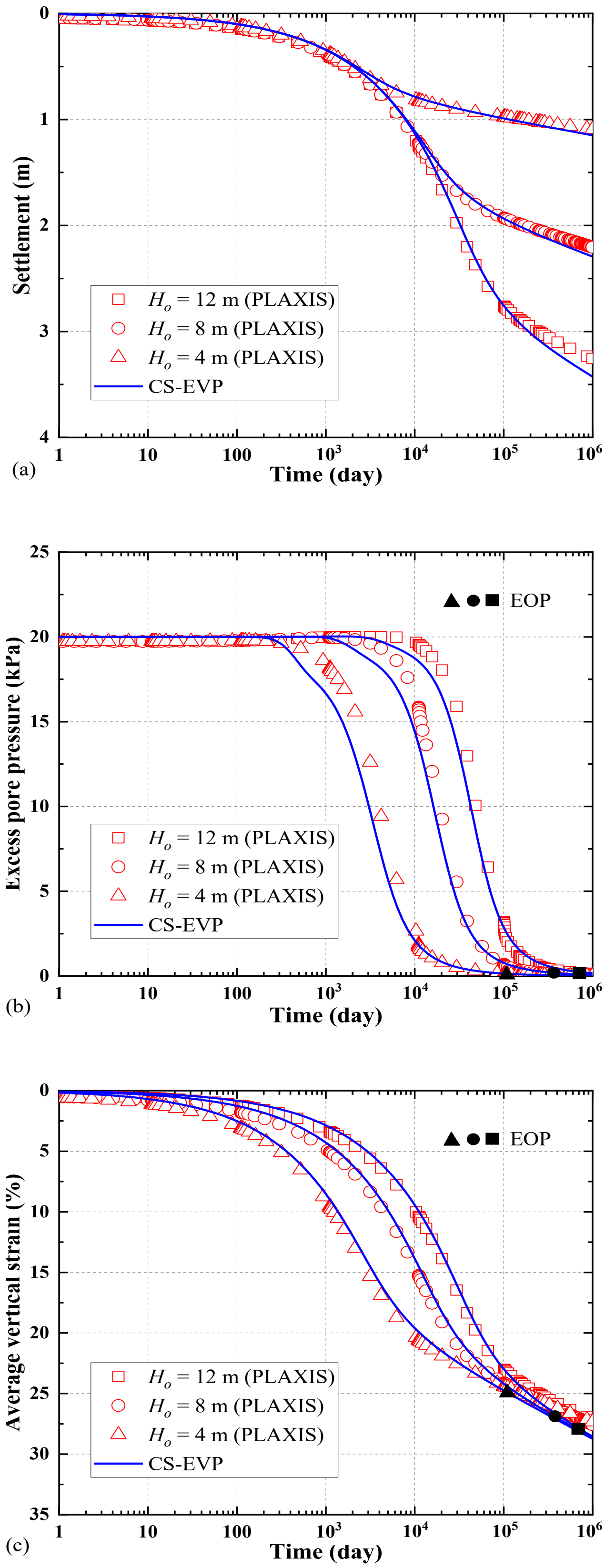

Fig. 6. Comparison of CS-EVP and PLAXIS simulation results for consolidation of single-layer columns: (a) settlement, (b) excess pore pressure at bottom boundary, and (c) average vertical strain

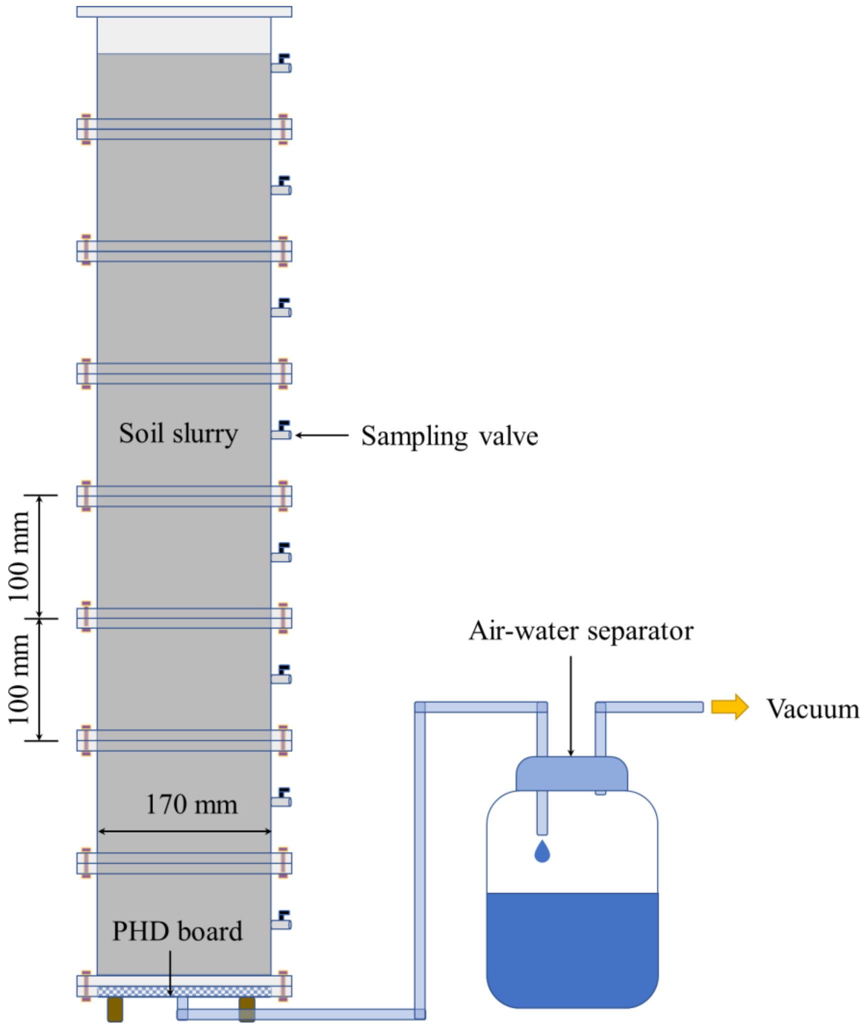

Fig. 7. Large-scale laboratory slurry consolidation test apparatus

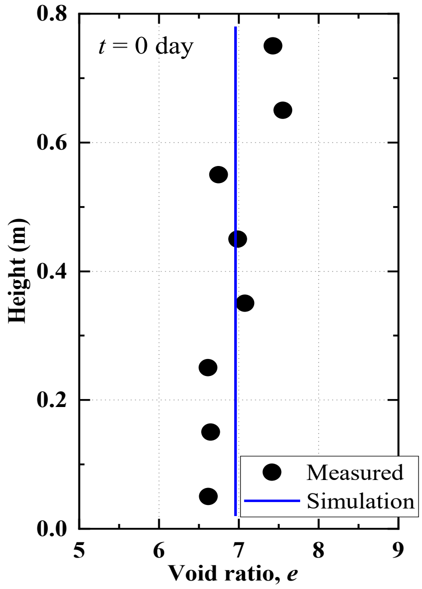

Fig. 8. Initial void ratio profile for laboratory slurry consolidation test

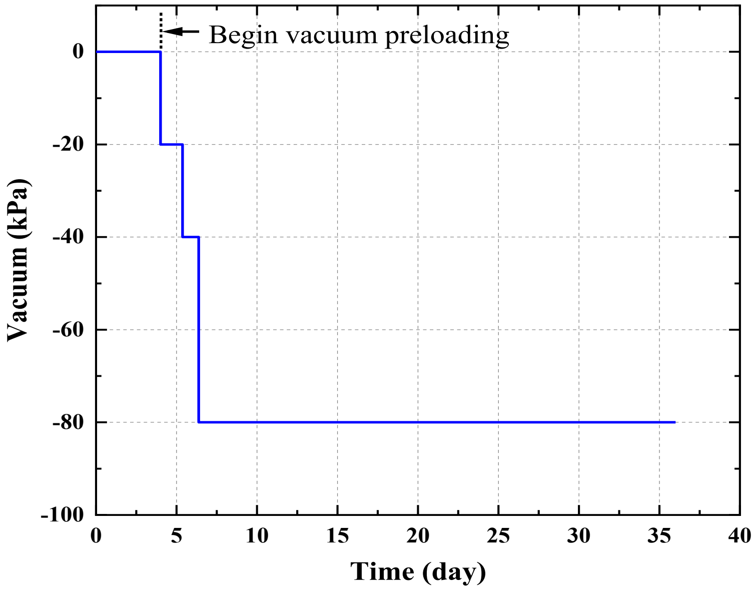

Fig. 9. Vacuum preloading schedule for laboratory slurry consolidation test

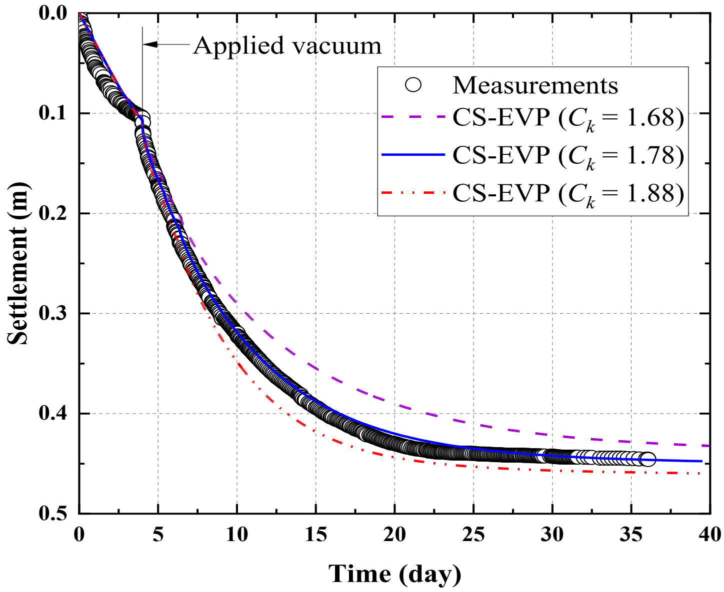

778

779 Fig. 10. Measured and simulated settlement relationships for laboratory slurry consolidation test

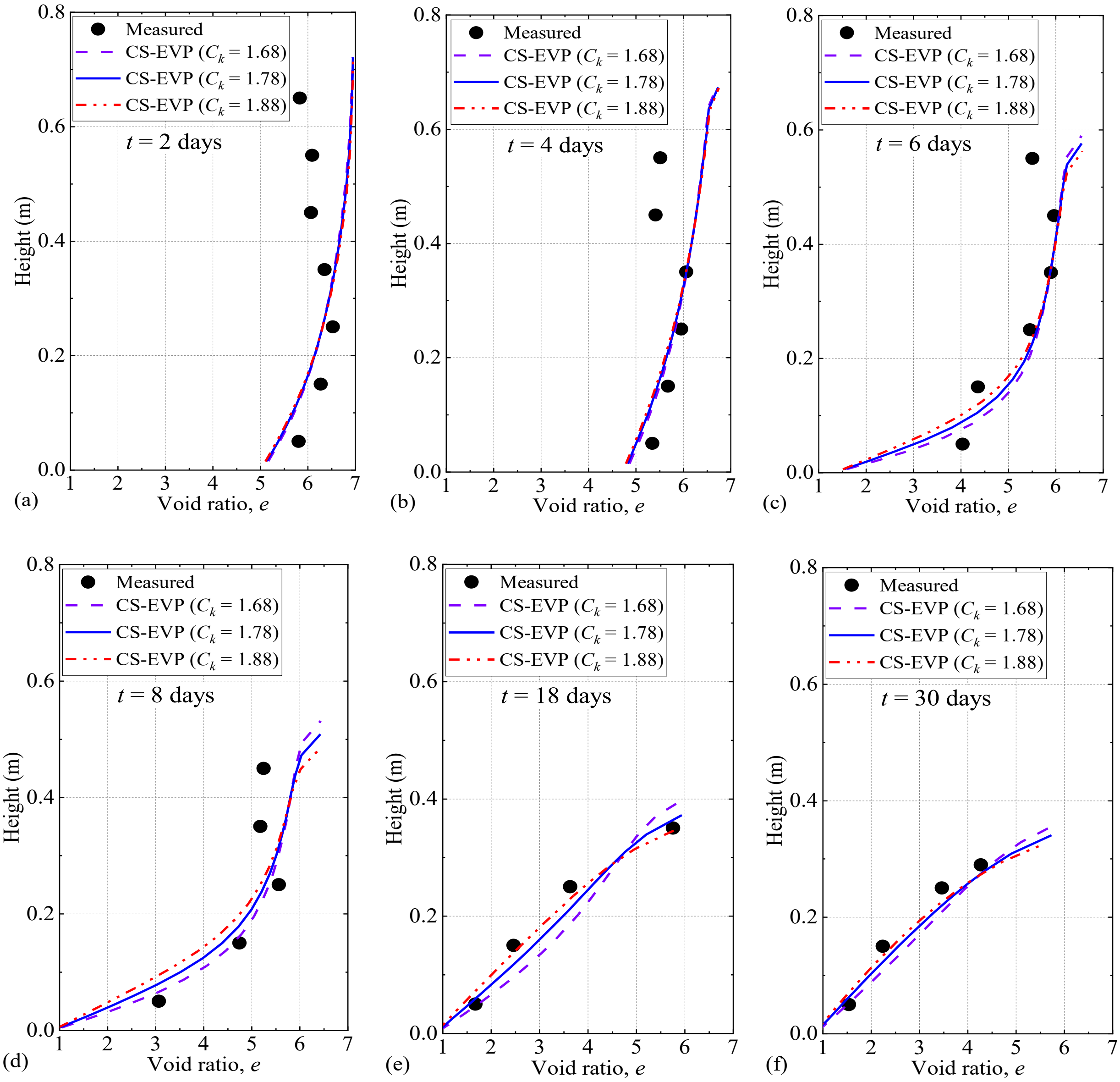

Fig. 11. Measured and simulated void ratio profiles for slurry consolidation test at: (a) t = 2 days, (b) t = 4 days, (c) t = 6 days, (d) t = 8 days, (e) t = 18 days, and (f) t = 30 days

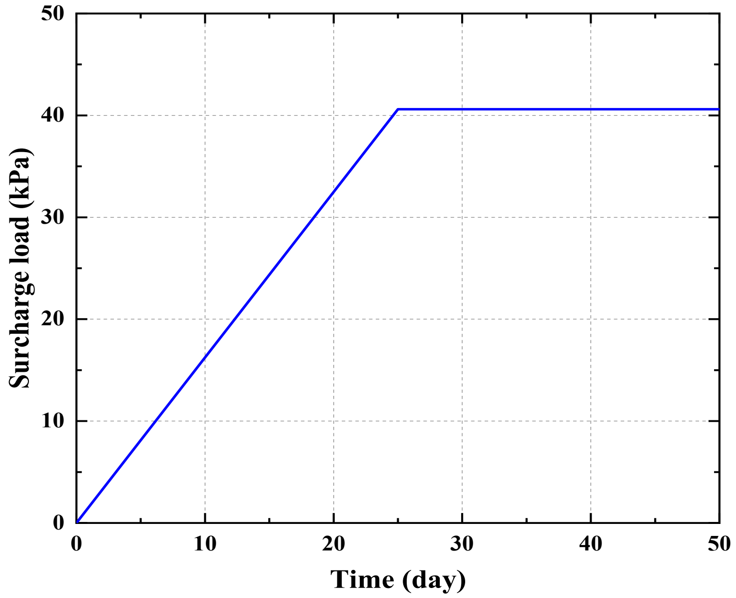

Fig. 12. Surcharge loading schedule for a test embankment at Väsby field site

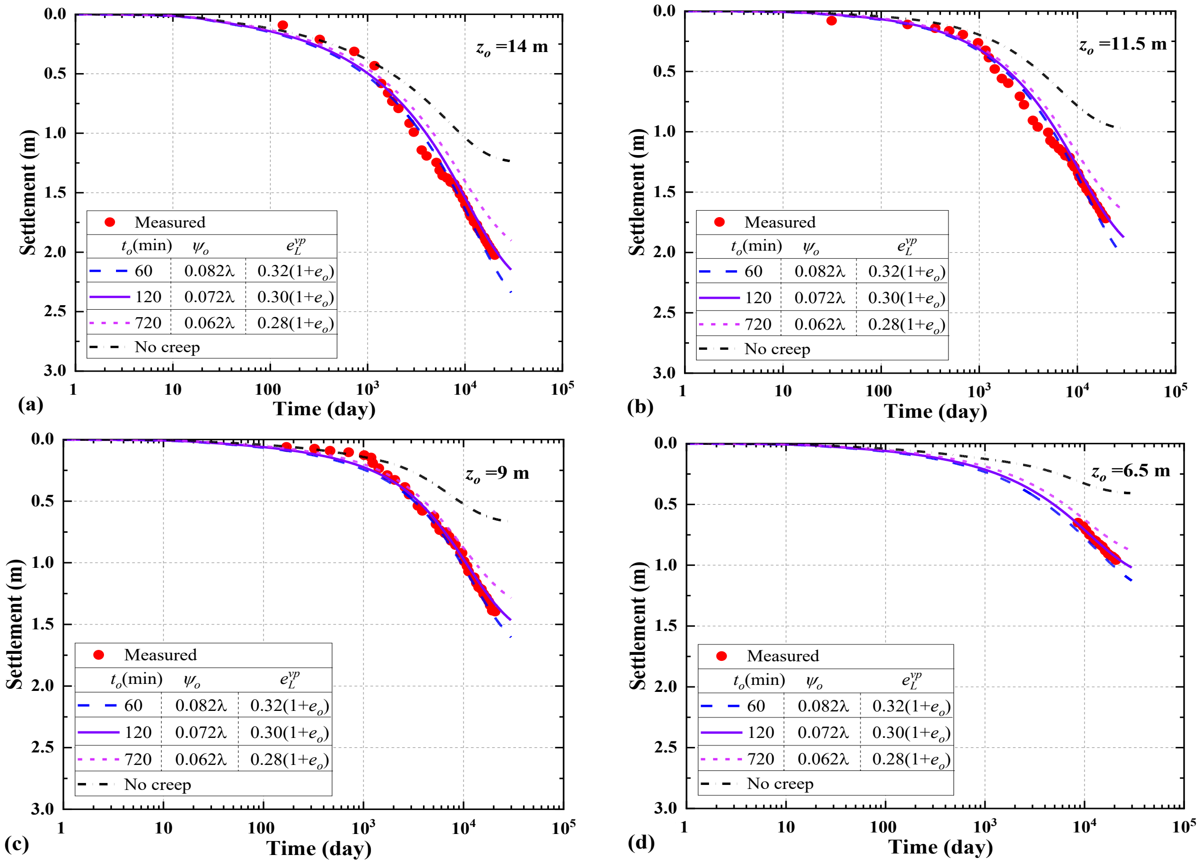

Fig. 13. Measured and simulated settlement relationships with time for a test embankment at Väsby field site: (a) z_o = 14 m, (b) z_o = 11.5 m, (c) z_o = 9.0 m and (d) z_o = 6.5 m

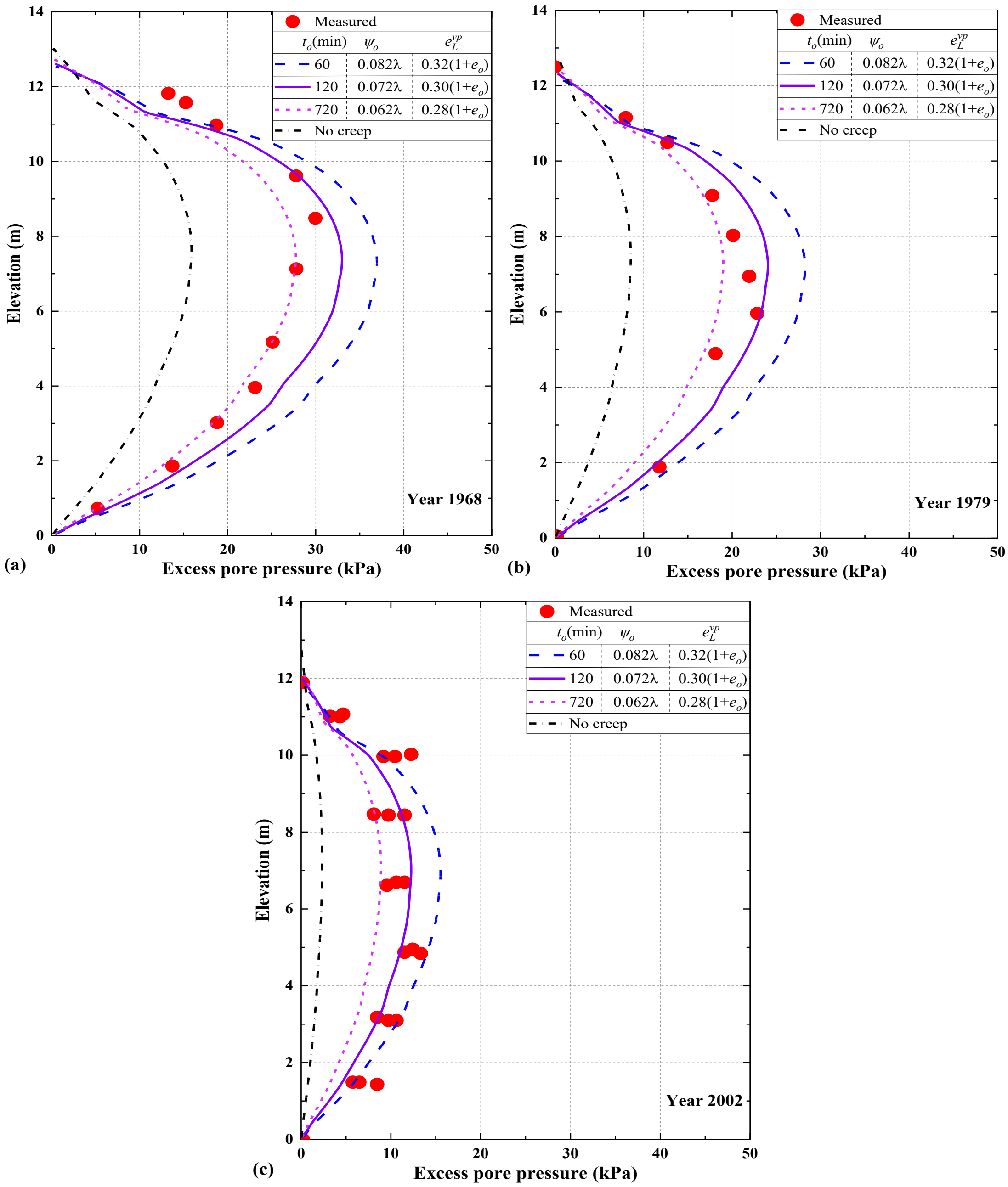

Fig. 14. Measured and simulated excess pore pressure profiles for a test embankment at Väsby field site: (a) year 1968, (b) year 1979 and (c) year 2002

Table 1. Soil parameters for consolidation analysis of a three-layer soil column

Layer No.	H_o (m)	κ	λ	ψ	e_o	σ'_o (kPa)	σ'_{ro} (kPa)	C_k	k_o (m/min)	t_o (min)
1	4	0.0005	0.161	0.059	1.88	1	10	0.8	3.63×10^{-7}	1440
2	4	0.0317	0.301	0.052	2.01	1	10	0.9	3.66×10^{-7}	1440
3	2	0.0548	0.269	0.058	2.48	1	10	1.1	3.15×10^{-7}	1440

Table 2. Soil properties for Hong Kong marine deposits

Property		Range of Values
Specific gravity of solids, G_s		2.59-2.68
Particle size distribution (%)	Sand	7.6-16.3
	Silt	58.8-63.7
	Clay	18.6-28.0
Liquid limit, w_L		59.9-67.7
Plasticity index, I_p		32.7-38.3
[a] Compression index, C_c		1.38-2.21
[a] Secondary compression index, $C_{\alpha e}$		0.01-0.03
[b] Hydraulic conductivity change index, C_k		0.9-1.9

[a] from oedometer test with loading range of 0.025 kPa to 100 kPa

[b] back-calculated value

Table 3. Soil properties for layered clays at Väsby test site (after Chen et al., 2021)

Layer No.	Elevation, z (m)	H_o (m)	κ	λ	e_o	σ'_o (kPa)	σ'_{ro} (kPa)	k_o ($\times10^{-8}$ m/min)	C_k
1	0-0.5	0.5	0.026	0.261	1.38	52.5	57	6.50	0.9
2	0.5-1.5	1.0	0.033	0.328	1.6	50.7	59.2	6.53	0.8
3	1.5-2.4	0.9	0.046	0.46	1.88	46.9	59.9	6.53	1.3
4	2.4-3.9	1.5	0.059	0.592	2.17	43.5	63.1	6.53	1.3
5	3.9-4.5	0.6	0.036	0.355	1.99	37.9	53.9	9.00	1.11
6	4.5-5.5	1.0	0.036	0.355	1.99	35.6	46.2	6.25	1.21
7	5.5-6.5	1.0	0.037	0.365	2.01	31.9	47.9	5.97	1.31
8	6.5-7.4	0.9	0.037	0.365	2.01	28.1	38.9	9.07	1.45
9	7.4-8.5	1.1	0.051	0.505	2.48	24.8	30.3	5.90	1.35
10	8.5-9.5	1.0	0.051	0.505	2.48	20.6	30.7	6.33	1.35
11	9.5-10.5	1.0	0.049	0.494	2.79	16.9	24.1	6.80	1.5
12	10.5-11.5	1.0	0.040	0.401	2.9	13.1	19.1	6.29	1.31
13	11.5-12.4	0.9	0.054	0.536	3.26	9.4	13.7	6.54	1.4
14	12.4-13.2	0.8	0.037	0.369	2.9	6	17.9	10.73	1.3
15	13.2-14.0	0.8	0.037	0.369	2.9	3	12.3	10.93	1.3